

Machine Vision-Based Assessment of Fall Color Changes in Apple Leaves and its Relationship with Nitrogen Concentration

Achyut Paudel^{a,*}, Jostan Brown^b, Priyanka Upadhyaya^a, Atif Bilal Asad^a, Safal Kshetri^a, Joseph R. Davidson^b, Cindy Grimm^b, Ashley Thompson^c, Bernardita Sallato^d, Matthew D. Whiting^e, Manoj Karkee^a

^aBiological Systems Engineering Department, Center for Precision and Automated Agricultural System, Washington State University, Prosser, 99350, WA, USA

^bCollaborative Robotics and Intelligent Systems Institute, , Oregon State University, Corvallis, 97331, OR, USA

^cMid-Columbia Agricultural Research and Extension Center, , Oregon State University, Hood River, 97031, OR, USA

^dIrrigated Agriculture Research and Extension Center, Washington State University, Prosser, 99350, WA, USA

^eDepartment of Horticulture, Washington State University, Prosser, 99350, WA, USA

Abstract

Apple (*Malus domestica* Borkh.) trees are deciduous, shedding leaves each year. This process is preceded by a gradual change in leaf color from green to yellow as chlorophyll is degraded prior to abscission. The initiation and rate of this color change are affected by many factors including leaf nitrogen (N) concentration. We predict that leaf color during this transition may be indicative of the nitrogen status of apple trees. This study assesses a machine vision-based system for quantifying the change in leaf color and its correlation with leaf nitrogen content. An image dataset was collected in color and 3D over five weeks in the fall of 2021 and 2023 at a commercial orchard using a ground vehicle-based stereovision sensor. Trees in the foreground were segmented from the point cloud using color and depth thresholding methods. Then, to estimate the proportion of yellow leaves per canopy, the color information of the segmented canopy area was quantified using a custom-defined metric, “*yellowness index*” (a normalized ratio of yellow to green foliage in the tree) that varied from -1 to +1 (-1 being completely green and +1 being completely yellow). Both K-means-based methods and gradient boosting methods were used to estimate the *yellowness index*. The gradient boosting based method proposed in this study was better than the K-means-based method (both in terms of computational time and accuracy), achieving an R^2 of 0.72 in

*Corresponding author.

Email address: achyut.paudel@wsu.edu (Achyut Paudel)

estimating the *yellowness index*. The metric was able to capture the gradual color transition from green to yellow over the study duration. Trees with lower leaf nitrogen showed the color transition to yellow earlier than the trees with higher nitrogen. The onset of color transition during both years occurred during the 29th week post-full bloom (October 22 in 2021 and Nov 10 in 2023). This critical timing could be used for conducting nitrogen status analysis on apple trees using machine vision, enabling more precise and timely assessment of nutrient levels and facilitating targeted fertilization strategies in orchard management.

Keywords: Leaf Color Change, Machine Vision, Point Cloud Segmentation, Precision Nitrogen Management, Machine Learning

1. Introduction

Water and nutrient applications in commercial tree fruit orchards are managed at a block or field level, providing treatment relatively uniformly to hundreds or even thousands of trees without considering the variability among individual trees. This homogeneous management of nutrients in tree fruit crops often leads to sub- and/or super-optimal inputs, with negative impacts on tree growth, fruit yield, and fruit quality (Klein et al., 1989; Neilsen et al., 2009). Managing these inputs at the individual tree level (i.e. addressing the unique needs of individual trees) is a promising concept for improving tree vigor, fruit yield and quality. However, managing orchards (Figure 1) at the individual tree level is challenging, particularly in terms of assessing the needs of individual trees and making precise management decisions. Each tree within an orchard is unique with its specific needs for water, nutrients, and other inputs (Aggelopoulou et al., 2010; James A. Taylor et al., 2007). For eg., Aggelopoulou et al. (2010) reported spatial variability with a coefficient of variation (CV) of up to 82% for bloom and 40% for yield within the same block. The variability among trees can be caused by multiple factors including spatial variation of soil properties like texture, depth, slope, or microbial activities, variation in microclimates within orchards, and differences in tree training and pruning (Aggelopoulou et al., 2010, 2011; Umali et al., 2012; Cho, 2010; Parkin,

1993). Effective nutrient management at the individual tree level could be possible if these multiple factors can be accurately assessed for each individual tree.



Figure 1: A representative high density apple orchard plantation in Prosser, Washington. The trees have been trained in a tall spindle architecture and spaced closely (4 foot) forming a highly dense planar “wall”.

Nitrogen (N) is a major macro nutrient needed by apple (*Malus domestica* Borkh.) trees given its fundamental roles in tree growth, canopy and crop development, and fruit quality (Sanchez et al., 1995; Neilsen and Neilsen, 2002). Traditionally, the most common approach farmers use to assess tree N status involves laboratory-based assessments of leaf tissue. These can provide a quantitative indicator of uptake, and when contrasted with a standard provide an estimation of sufficiency (Marschner, 2011). Soil chemical testing of nitrate (NO_3^-) or ammonium (NH_4^+) availability, on the other hand, is not a reliable method to determine N supply, given its variability across the season and multiple forms of losses (Fox and Piekielek, 1978). These destructive methods demand significant time for sampling and their high cost limits the sampling density to few trees or locations, a practice that lacks precision due to inherent spatial variations within orchards (Ferguson and Triggs, 1990; Wulfsohn et al., 2012;

[Arnó et al., 2017](#)).

In addition to laboratory-based tests, experienced farmers and researchers often employ visual assessment of canopy features such as shoot length, canopy density, trunk diameter, overall tree growth, crop load, and leaf color to estimate N status.. While these observational methods leverage professional expertise, they suffer from subjectivity, and potential variability among assessors. The reliance on seasoned professionals further limits its widespread applicability in commercial orchards.

These limitations of both laboratory-based methods and visual assessments by subject matter experts underscore the need for a rapid, reliable, and more comprehensive approach to N status evaluation ([Cheng and Schupp, 2004](#)) at the individual tree level. A promising alternative is a machine-vision system that automates and standardizes the quantification of visual parameters across entire orchards. This approach could provide objective, empirical data that may be correlated with tree nitrogen status through modeling methods. By enabling more precise, tree-level management in commercial orchards, such a system has the potential to overcome the sampling and subjectivity issues inherent in current methods while offering scalability for broader applications.

Machine vision techniques have been extensively used to evaluate various canopy-level features and detect canopy stresses in fruit crops ([Wang et al., 2023](#); [Paudel et al., 2022](#); [Wachs et al., 2010](#); [Wang et al., 2018](#); [Brown et al., 2024](#)). More specifically, many recent studies have reported machine vision-based tools for estimating canopy density([Mahmud et al., 2021](#); [Paudel et al., 2023](#)), tree trunk cross-sectional area ([Wang et al., 2023](#)), and canopy color ([Naschitz et al., 2014](#)) in fruit trees.

Leaf color is one of the key canopy characteristics that is correlated with nitrogen content([Ali et al., 2012](#); [Treder et al., 2016](#); [Ye et al., 2020](#)). This correlation is due to the presence of four rings of N in the chlorophyll, the pigment in leaves responsible for light harvesting([Marschner, 2011](#)). Chlorophyll reflects light primarily in the green spectrum, which

is why plant tissue containing chlorophyll appears green. In deciduous trees like apples, a significant color change occurs from green to yellow as the growing season progresses towards fall, as the chlorophyll breaks down and mobile elements like N move back into the perennial structures of tree. This relocation of nitrogen from leaves to woody regions for storage will later support next seasons' growth(Murneek and Logan, 1932; Spencer, 1973; Neilsen and Neilsen, 2002).A greener canopy with vigorous growth is often correlated with a tree having high nitrogen, while a yellower and less vigorous canopy is often associated with trees with low nitrogen (Raese et al., 2007; Lee, 2002). In addition, trees with high nitrogen tend to maintain their green color longer into the season providing a potential indication of tree nitrogen status during this critical transition.

Various RGB, multispectral, and hyperspectral imaging techniques have been evaluated to quantify the color and estimate nitrogen or chlorophyll content in apples (Campbell et al., 1990; Neilsen et al., 1995; Perry and Davenport, 2007). Most of these studies use devices like chlorophyllmeter (SPAD) or satellite images. While handheld devices like SPAD meters can be utilized in the field, they pose challenges for scaling assessments across entire orchards due to the need for data collection from individual leaves. On the other hand, satellite imagery offers broader insights but often lacks the resolution required to pinpoint individual trees, necessitating further computations for accurate matching. Our study overcomes these limitations by focusing on individual tree-level assessments, providing a scalable and efficient approach for evaluating apple tree health and productivity in orchards.

In this study, we investigated the relationship between N status and color degradation utilizing RGB-D camera during apple tree senescence, . and explored the potential to utilize this assessment for precision management practices at the individual tree level.

Specifically, the study had the following two objectives:

1. Develop a machine vision-based technique to quantify foliage color during late fall in an apple orchard.

- Use the foliage color as an indicator to differentiate between trees with varying foliage leaf nitrogen concentration.

2. Materials and Methods

RGB-D images were collected over several weeks in fall of 2021 and 2023. These images were collected in a Jazz™ commercial orchard (Yakima Valley Orchard) near Prosser, WA, USA (Figure 3). The trees were trained to a vertical structure using a tall spindle canopy architecture (Figure 1). The point clouds of the tree canopies were then segmented into yellow and green foliage; a quantitative metric, termed the *yellowness index*, was created to estimate the color of the trees. The yellowness indices of the trees during different weeks were then correlated with the leaf nitrogen content for each year. The overall data collection and processing method used in this study is shown in Figure 2.

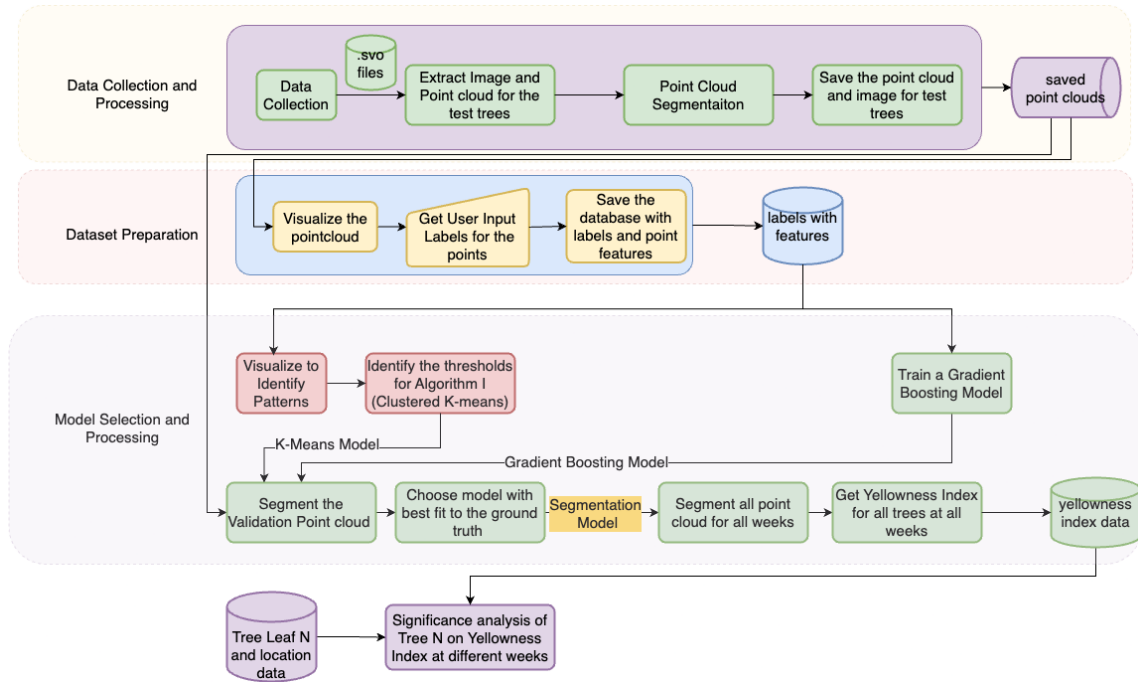


Figure 2: Overall data collection and processing steps used in the study; Each light-colored box represents a distinct process and has been described further in the subsequent sections.

2.1. Data Collection

The datasets (color and 3D images) for this study were collected over five weeks in fall, 2021 (from October 13 to November 14) and fall, 2023 (from October 20 to November 17), every week. The first image datasets were determined by when the leaves began to change color from green to yellow (Figure 4), The dataset was collected from a total of 200 trees across 17 rows of the test orchard, with every other 3rd tree in each row taken as a sample. The data were collected using a commercial stereovision-based RGB-D camera (Zed2i, Stereolabs, Paris, France) mounted on a utility vehicle (Figure 3b). The camera was mounted 2 meters above the ground to ensure that most of the canopy (Figure 4, part of tree above 0.3m from ground) was visible. An SVO file (Stereolabs file format) with all the metadata including the camera parameters, images, and sensor data was recorded for each row of trees. Images (pixel resolution of 2208 x 1242) and point clouds (maximum depth of 10m) for each tree were later extracted based on timestamp matching between frames and user input. During processing, the RGB and co-registered point cloud were identified for each test tree.

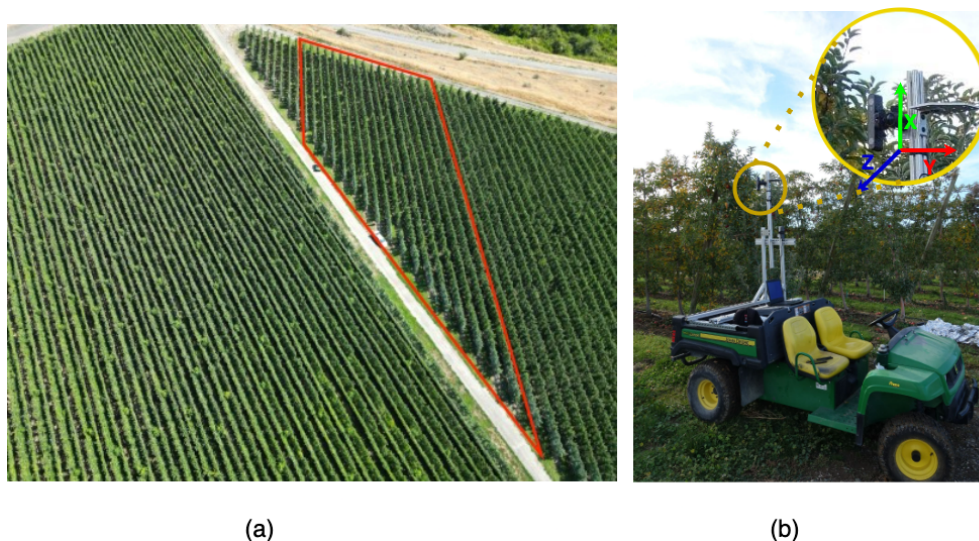


Figure 3: Study site and sensing setup; (a) An aerial view of the test plot. The red outline shows the location of the plot used in this study., and b) Ground vehicle with a camera mounted on top (zoomed portion shows camera and axes orientations)

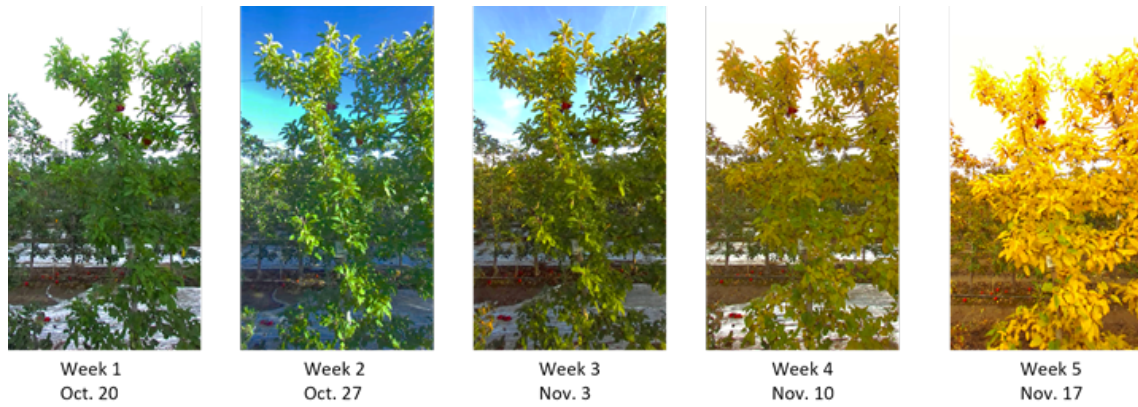


Figure 4: Images of a sample apple tree acquired over the data collection period in 2023. The foliage can be seen gradually changing from green to yellow.

2.2. Point Cloud Processing and Segmentation

2.2.1. Foreground Tree Segmentation

The initial data acquired through the stereovision sensor were noisy and required further refinement. An initial step involved applying a color threshold of 153 to the blue channel to filter out pixels corresponding to the sky in the RGB color space. Subsequently, a distance threshold of 3 meters along the Z-axis (depth axis), was implemented. The optimal threshold values were determined experimentally through trials and visual inspections. Consequently, the resulting point cloud consisted of points mostly from the foreground tree, with some residual points from the ground. To eliminate the undesirable ground points, the points within 50 centimeters above the lowest x-value (along the height of the tree) were excluded. The resulting point cloud was down-sampled by selecting every tenth point, effectively reducing its size while preserving essential information for subsequent analysis.



Figure 5: Schematic for point cloud segmentation and downsampling process used in the study

2.2.2. Color Segmentation and Clustering

The point cloud obtained from step 2.2.1 consisted of points from the foreground tree, and could be broadly categorized into yellow leaves, green leaves, and the trunk. To quantify the color changes in trees' over the duration of study, HSV (Figure 6a) and CIE-Lab* (Figure 6b and 6c) color spaces were used as they are less affected by the variation in intensities. In the HSV space, hue remains unaffected by varying light intensity, while in the CIE-Lab* space, the a^* and b^* values correspond respectively to red-green and blue-yellow colors. RGB images captured by the RGB-D sensor were converted to both the CIE-La*b* (Lab) space, using a standard D65 illuminant, and the HSV color space. These conversions were performed using the scikit-image library (Van der Walt et al., 2014).

The transition of the trees from green to yellow color was noticeable in both HSV and La*b* space (Figures 6a and 6b,c). A probability density plot for the hue space across the weeks illustrated a decline from approximately 110 degrees in week 1 to about 50 degrees in week 6 (hue expressed as degrees between 0 and 360, as shown in Figure 6a), signifying the shift from green to yellow. A similar trend was visible in the probability density plots for a^* and b^* in the La*b* space. Both a^* and b^* showed a slight increase as the weeks progressed, corresponding to a color change from green to yellow.

The transition in tree canopy color was apparent qualitatively, but a robust quantitative approach was needed to precisely quantify them. To achieve this, individual points in the point cloud were categorized into distinct groups of yellow leaves, green leaves, or the trunk. Qualitative analyses using K-means clustering over multiple samples in both the La*b* and HSV color spaces showed that the La*b* space performed better in distinguishing yellow and green pixels as separate classes. Consequently, the subsequent analysis was conducted using La*b* color space. To cluster the point cloud, a modified k-means algorithm (Algorithm 1) was applied, initially grouping the points into 20 clusters. A threshold for the cluster center was set in both the a^* and b^* space, to merge these clusters into three distinct classes:

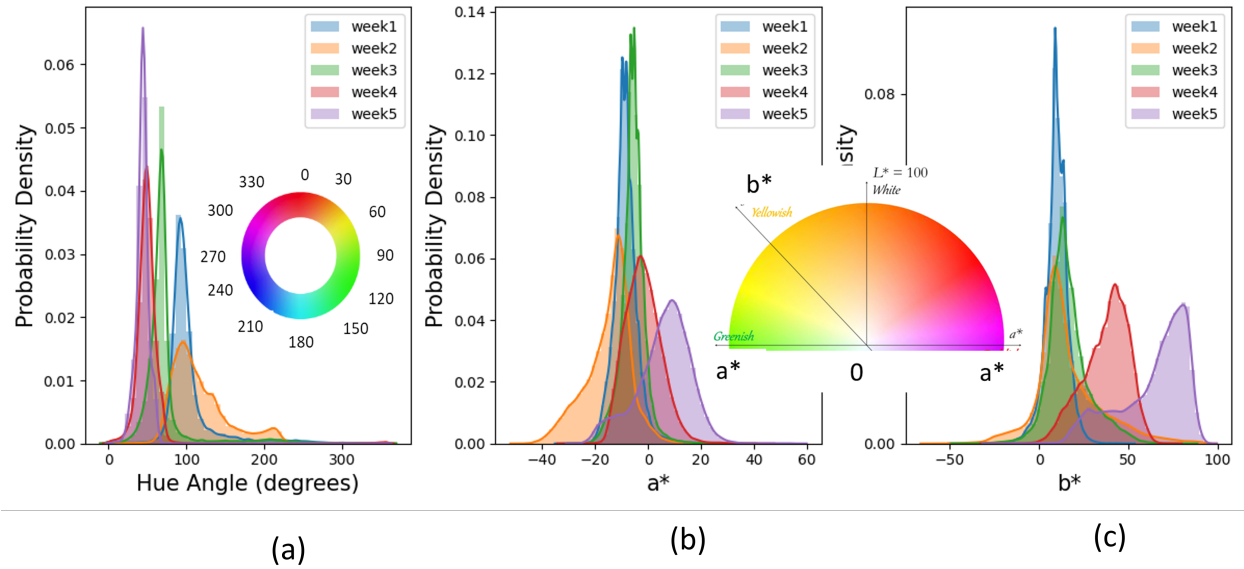


Figure 6: Distribution of a) Hue angles and b) a^* and c) b^* values for one of the sample trees during the five-week study period of 2023. The color chart shows the color associated with different values for (a) hue angles, (b) (Thompson, 2017) a^* , and b^* . The hue angle decreased in a) and a^* and b^* increased in b) and c) as the weeks progressed during the study all signifying the shift from green to yellow.

Yellow, Green, and Trunk. The *Yellow* cluster encompassed foliage that had transitioned to yellow, while the *Green* cluster comprised foliage that retained its green color. The *Trunk* cluster included points from the trunk, branches, background soil, and some brown leaves. A detailed breakdown of the clustering process is outlined in Algorithm 1.

Algorithm 1: Clustering of Point Cloud based on a^* , b^* values

Input: Point cloud from stereovision system, P

Output: Clustered Point cloud–3 groups: Green (c_g), Yellow (c_y), Trunk (c_t)

```
1 Define  $n$  as the initial number of clusters (integer)
2 Perform K-Means clustering using  $a^*$ ,  $b^*$  values into  $n$  clusters ( $C = \{c_1, c_2, \dots, c_n\}$ )
3 Initialize Green cluster ( $c_g$ ), Yellow cluster ( $c_y$ ), and Trunk cluster ( $c_t$ ) as empty sets:

4  $c_g = \emptyset$ ;  $c_y = \emptyset$ ;  $c_t = \emptyset$ 
5 Define  $a^*$  and  $b^*$  thresholds for Green cluster:  $[cg_{amin}, cg_{amax}]$ ,  $[cg_{bmin}, cg_{bmax}]$ 
6 Define  $a^*$  and  $b^*$  thresholds for Yellow cluster:  $[cy_{amin}, cy_{amax}]$ ,  $[cy_{bmin}, cy_{bmax}]$ 
7 Define  $a^*$  and  $b^*$  thresholds for Trunk cluster:  $[ct_{amin}, ct_{amax}]$ ,  $[ct_{bmin}, ct_{bmax}]$ 
8 for  $i \in \{1, 2, \dots, n\}$  do
9   if  $cg_{amin} \leq c_i(a) \leq cg_{amax}$  and  $cg_{bmin} \leq c_i(b) \leq cg_{bmax}$  then
10      $c_g = c_g \cup c_i$ 
11     // Merge cluster  $c_i$  into Green cluster
12   else if  $cy_{amin} \leq c_i(a) \leq cy_{amax}$  and  $cy_{bmin} \leq c_i(b) \leq cy_{bmax}$  then
13      $c_y = c_y \cup c_i$ 
14     // Merge cluster  $c_i$  into Yellow cluster
15   else if  $ct_{amin} \leq c_i(a) \leq ct_{amax}$  and  $ct_{bmin} \leq c_i(b) \leq ct_{bmax}$  then
16      $c_t = c_t \cup c_i$ 
17     // Merge cluster  $c_i$  into Trunk cluster
18   end
19 end
20 return  $c_g, c_y, c_t$ 
```

In the aforementioned algorithm, the manual setting of threshold values for a^* and b^* required multiple iterations to identify optimal values suitable across the data throughout

the weeks. To standardize this process, a methodology involving manual user input labels was implemented to obtain a labeled dataset. A custom Python program (Figure 7), using the Open3D library (Zhou et al., 2018), was developed to label the point cloud. This interactive program allowed users to choose between three labels - 'Green', 'Yellow', and 'Trunk' and manually select the points belonging to these labels. Trees were randomly sampled throughout the entire data collection period, and the labels along with the characteristics of the points were recorded to create the dataset.

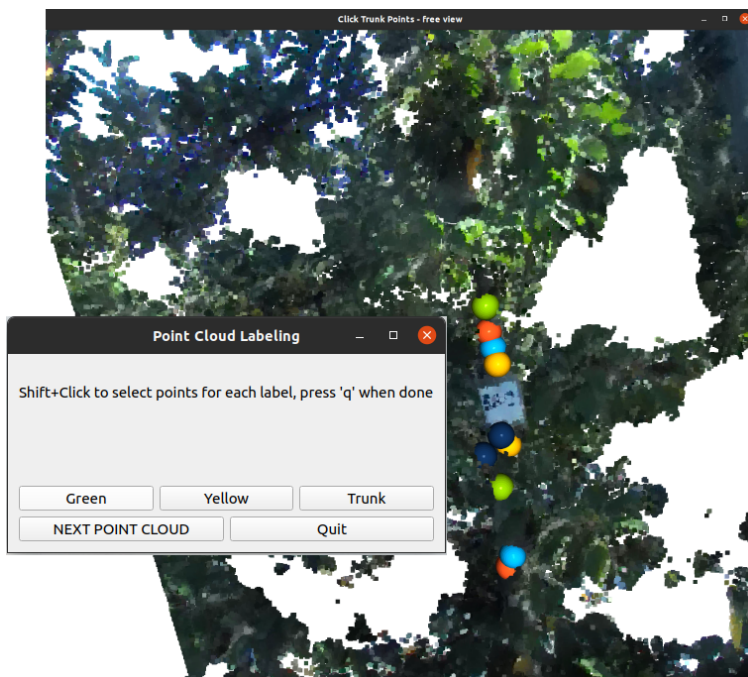


Figure 7: A custom program to select the points belonging to multiple classes - Green, Yellow, and Trunk. This instance showed an interactive window where the user selected points belonging to the trunk. The features of the points - including a^* , b^* , R , G , B , and their eigenvector and eigenvalues (in a neighborhood) were recorded into a spreadsheet for further analysis.

To visualize the difference between groups, a distribution plot of the a^* , and b^* spaces was created (Figure 8). These plots provided strategic reference points for selecting threshold values. For the 2023 dataset, the threshold values for a^* and b^* were determined as follows: $a^* < -10$, $0 < b^* < 25$ for *Green*, $b^* > 45$ for *Yellow*, and $a^* > 0$, $0 < b^* < 50$ for *Trunk*. While K-means clustering, being an unsupervised method, doesn't necessitate user inputs for training data and attempts to identify inherent clusters in the dataset, it comes with

certain drawbacks. The method’s main limitations include longer computation times due to the need to process all points and its reliance on random initialization, potentially leading to different solutions with each run.

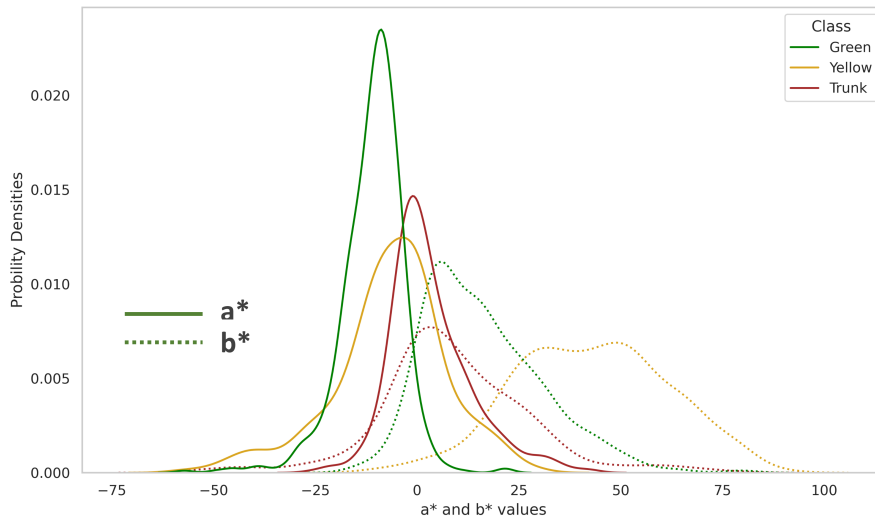


Figure 8: a^* and b^* values in CIE- $L^*a^*b^*$ space during different weeks of image acquisition (2023) for points belonging to green, yellow, and trunk classes. The solid lines represent a^* values, and dotted lines represent b^* values, different colors represent different classes.

An alternative approach utilized a gradient boost classifier, an ensemble learning technique that combines multiple weak learners (typically decision trees) to create a stronger, more robust model (Bartlett et al., 1998).. It sequentially builds new models, focusing on correcting the errors made by the previous ones, ultimately producing a more accurate and powerful predictive model (Natekin and Knoll, 2013). In this study, the gradient boost classifier model was created using scikit-learn (Van der Walt et al., 2014). The dataset was divided into 80% training and 20% testing sub-sets. The model required tuning of different hyperparameters. A strategic approach to varying model hyperparameters was employed, with one hyperparameter held constant while varying the others to analyze their individual effects on model accuracy. The hyperparameter learning rate was varied between 0.1-1, max depth was varied between 1-5, and n estimator was varied between 100-1000 and their performance on training and test dataset was analyzed. The set of hyperparameters that

achieved the highest accuracy on the test data was then selected.

The outputs from both Algorithm 1 (K-Means) and the Gradient Boosting method provided labels—'Green', 'Yellow', or 'Trunk'—for each point in the point cloud. Following the clustering of points, a metric, *yellowness index*, was used to quantify the extent of yellowing within each tree canopy. The *yellowness index*, calculated using Equation 1, represents the normalized ratio between yellow and green points within a tree canopy, with values ranging between -1 and +1. A value of -1 indicates that the tree was entirely green, while a value of +1 signifies complete yellowing.

$$\text{yellowness index} = \frac{y-g}{y+g} \tag{1}$$

where,

y = number of points with 'Yellow' label (c_y)

g = number of points in 'Green' label (c_g)

To assess the performance of the yellowness estimation techniques, 50 validation trees were randomly selected and defoliated between the second and fourth trellis wires (a section of the trees, Figure 9). The leaves removed from each tree were collected in a bag and then later segregated manually into separate groups (“Green” or “Yellow”) for each tree. A leaf was identified as 'Green' if more than half of the leaf area was green, and 'Yellow' if otherwise. The precise weights of the yellow and green leaf groups were measured using a highly accurate Mettler PC 4000 (Mettler Toledo, Switzerland) weighing scale. This value served as the ground truth to assess the models' performance. The *yellowness index* value was computed for all validation trees using Equation 1. Both Algorithm 1 (K-means) and Gradient Boosting were evaluated against the ground truth data, with the superior-performing model based on this evaluation selected for further study. A timing test was also performed to evaluate the computation time of each of the model. Both models were run on a System76 Oryx

Pro (System76, Inc., Colorado, USA) equipped with 16GB RAM, an 8GB NVIDIA GeForce RTX 3070 GPU (NVIDIA Corp., California, USA), and an Intel i7-11800H processor (Intel Corp., California, USA) at 2.30 GHz with 16 cores.



Figure 9: Images of a sample tree before and after deleafing. The leaves of 50 sample trees within a section between the second and fourth trellis wire were removed (shown in transparent red box) and collected to estimate the ground truth *yellowness index*.

2.3. *Yellowness Index and Leaf Nitrogen Concentration*

To investigate if the *yellowness index* had any relationship with the foliar nitrogen concentration on the trees, the *yellowness index* values were regressed against the leaf nitrogen concentration. The leaf nitrogen concentration was obtained using the standard Kjeldahl's method(Kirk, 1950) by collecting 50 fully grown mid-shoot leaves from each tree, at the end of the growing season (Late July in 2021 and early August in 2023). The leaf nitrogen concentration represents the average leaf nitrogen concentration of each tree and is associated with canopy growth and canopy color. The leaf nitrogen level of 2-2.4% was regarded as an adequate range for nitrogen concentration based on referenced values for apples(Cheng and Schupp, 2004; Cheng, 2010; Sallato, 2017; UniversityofArizona).

A one-way ANOVA was performed to examine differences in the yellowness index among trees. This analysis was conducted separately for each week of the season, comparing trees grouped by their leaf nitrogen levels to determine if trees with different nitrogen statuses exhibited significant variations in their yellowness index throughout senescence. The trees

were classified into 5 groups according to their leaf nitrogen concentrations: 'VeryLow' ($N < 1.7\%$), 'Low' ($1.7\% < N < 2\%$), 'Good' ($2\% < N < 2.4\%$), 'High' ($2.4\% < N < 2.6\%$), and 'VeryHigh' ($N > 2.6\%$). The ANOVA analysis was followed up by a Tukey HSD posthoc analysis to analyze the significant difference between pairs of groups if ANOVA showed a significant difference between those groups.

3. Results and Discussions

3.1. Tree Segmentation and Clustering

The original color point cloud was clustered into green and yellow groups to quantify the yellowness of each tree canopy in the test orchard. As discussed in the methods section, Algorithm 1 (K-means based) and the Gradient Boost classifier were used to classify leaves into these two groups. For the Gradient Boost model, *learning rate*, *max depth*, and *n estimator* were varied to identify the best set of hyperparameters (Figure 11). The model started to overfit the training data on increasing the hyperparameters, as indicated by higher performance on the training set with reduced performance on the test set (e.g., training accuracy went from 0.85 to nearly 1, while testing accuracy decreased as *max_depth* of the trees was varied from 1 to 3, Fig 10b). The gradient boost method with the best set of hyperparameters achieved an accuracy of 78% on the test set with a *learning rate* of 0.1, *maximum depth* of 1, and *number of estimators* as 100.

Using the validation data (detailed in Section 2.2.2), the Gradient Boost model, with the optimal hyperparameter configuration, was compared against Algorithm 1. Figure 11 qualitatively shows the performance of the two models within the cropped canopy regions (between the second and fourth trellis wire). Quantitative assessment of the performance of these models was performed using the Yellowness Indices (calculated with the proposed method as well as the manual estimation in the field) of the validation trees (Figure 12). Both models were similar in their classification accuracy on the validation dataset with R^2 of 0.69 for Algorithm 1 and 0.72 for gradient boost model. This suggests there is a good

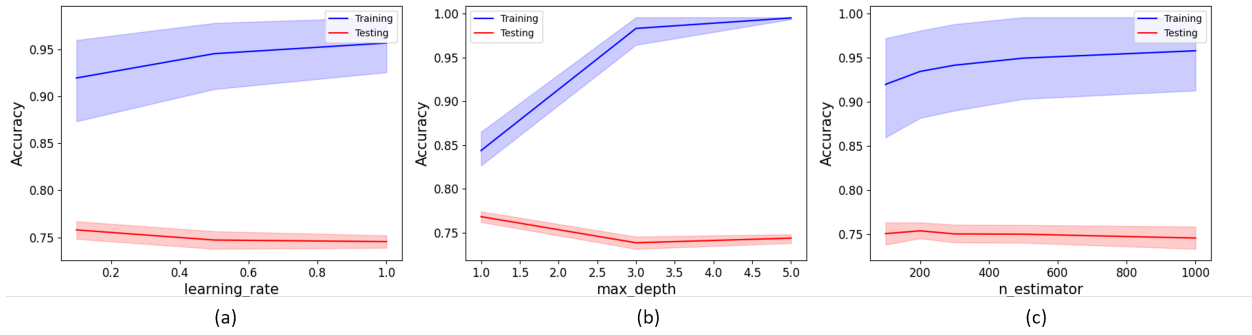


Figure 10: Varying accuracies for the gradient boost model with different combination of hyperparameters (a) Learning Rate, b) Maximum Depth of Tree, and c) Number of Estimators. The blue line denotes varying accuracy during training whereas the red line represents varying accuracy during testing. The shaded regions around the lines illustrate the range of accuracies across different values of the other hyperparameters, with the indicated hyperparameter being held constant.

fit between the ground truth (Yellowness indices of the validation trees) and calculated yellowness. However, Algorithm 1 had significantly slower processing speeds compared to the Gradient Boost method. On the same point cloud, the Gradient Boost model was approximately six times faster (with average segmentation time of 0.39 sec per tree) compared to Algorithm 1 (2.41 sec per tree). Consequently, Gradient Boost was used for subsequent point cloud segmentations. Figure 13 demonstrates the results from the gradient boost segmentation model for a test tree during weeks 1, 3, and 5.

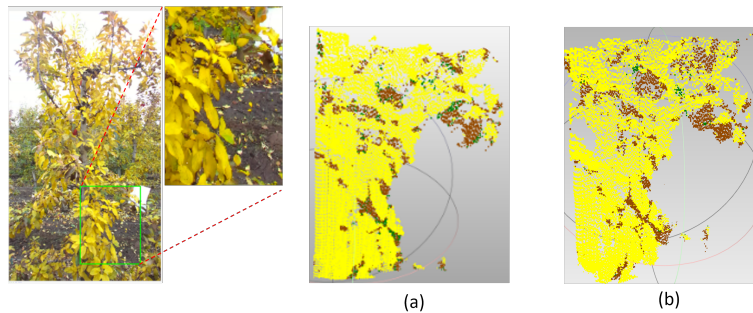


Figure 11: Example segmented point cloud of tree canopies in the validation data. The region delineated by the green rectangle was cropped and the corresponding color image and point cloud data was extracted for performance assessment. The results from the segmentation models on the cropped point cloud are shown in a) Algorithm 1; and b) Gradient Boost Classifier. The three colors in the point cloud represent three groups; green leaves, yellow leaves, and trunk.

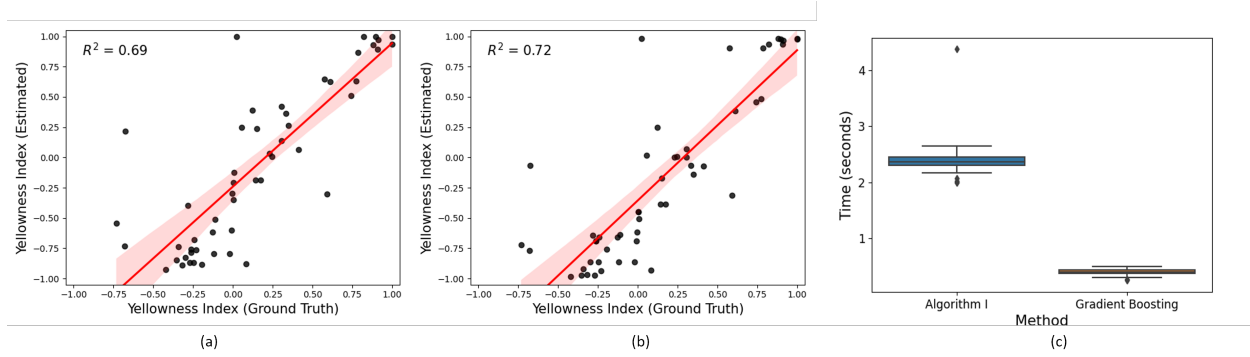


Figure 12: Relationship between estimated and manually calculated yellowness index for two classification/clustering models on the validation dataset; estimated vs ground truth *yellowness index* achieved by a) Algorithm 1; b) Gradient Boost; and c) Processing time (per image) on thirty-five test trees across all five weeks of data collection in 2023.

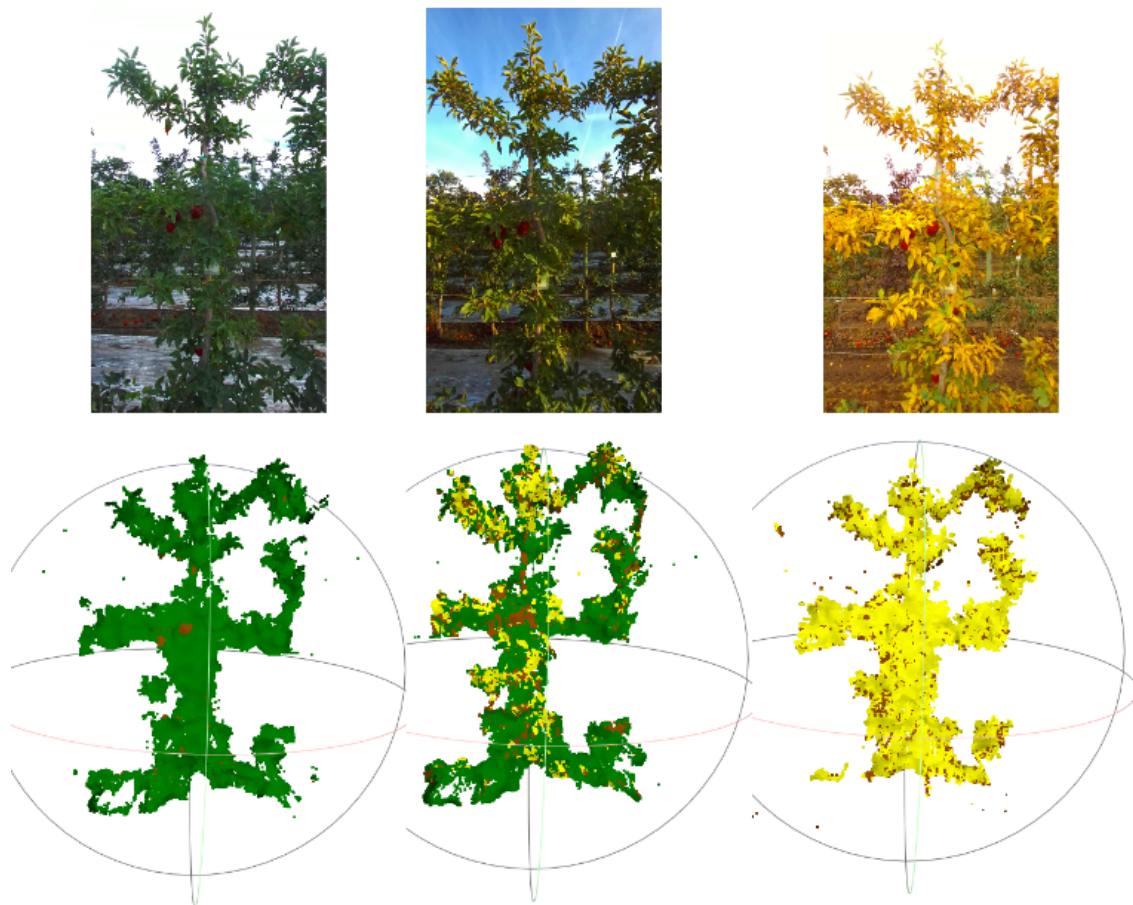
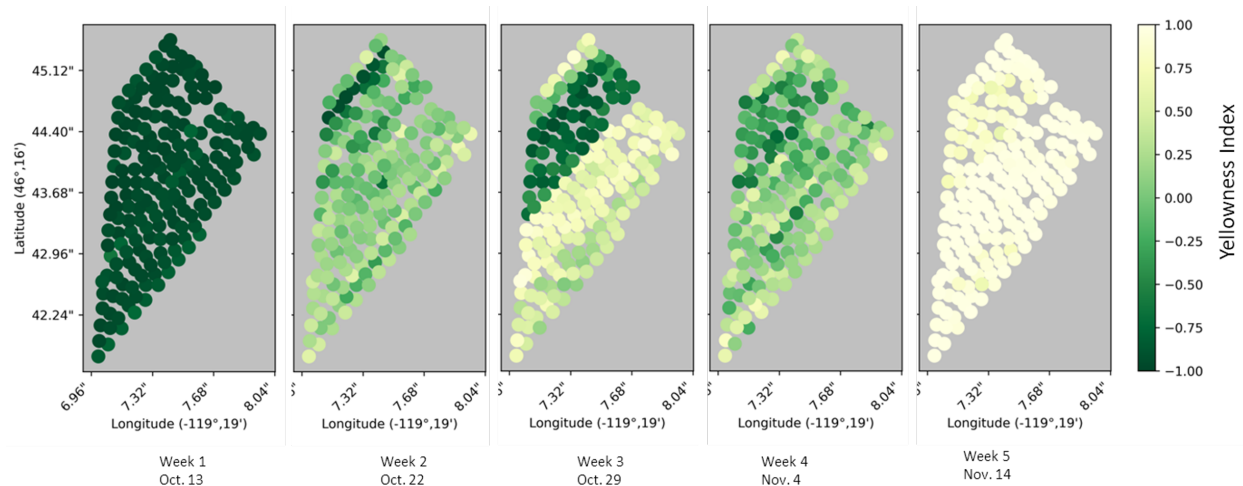


Figure 13: The images (top row) and segmented point cloud (bottom row) of a test tree during weeks 1,3, and 5. The three colors in the point cloud represent three groups; green-green leaves, yellow-yellow leaves, and brown-trunk, branches and some leaves that have turned brown.

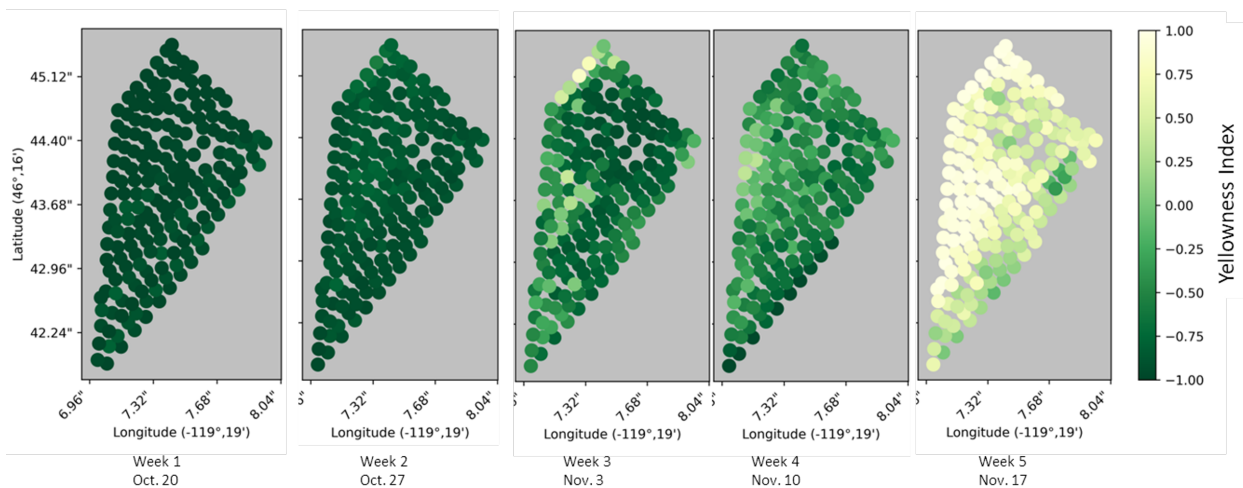
3.2. *Yellowness Index and Leaf Nitrogen Concentration*

The segmented point clouds were used to calculate the *yellowness index* for each tree over individual weeks using equation 1. The pattern and progression of yellowing of trees is depicted in spatial maps of these yellowness indices during fall 2021 (Figure 14a) and fall, 2023 (Figure 14b). The darker points in these maps represent greener trees and the lighter points represent trees with more yellow leaves. In both years we recorded a consistent increase in *yellowness index* over time. However, the progression of yellowing was different between the two years. In 2021, trees began the transition to yellow in week 2 (around October 22), whereas in 2023, this change occurred later in the year after November 10. This difference may be due to relatively higher temperature during the growing season in 2021 compared to 2023 (AgWeatherNet). Comparing years in growing degree days (GDD) provides a more precise measure of plant growth stages than calendar days, as GDDs account for the variable influence of temperature on developmental rates, allowing for more accurate predictions of phenological events regardless of annual temperature fluctuations (Dass and Rai, 2013). Prior studies by De la Haba et al. (2014) and Kim et al. (2020) have demonstrated that elevated temperatures can induce early senescence in foliage. In our research site, the timing of full bloom in 2021 was almost three weeks earlier than 2023. This difference in bloom correlates with the observed variations in the timing of tree yellowing, and further highlights the role of temperature influencing key phenological stages. In both years, yellowing occurred approximately 29 weeks after full bloom.

The correlation between leaf nitrogen concentration and yellowness index was determined for each week in 2021 and 2023 (Figure 15). The trees were categorized into five groups based on their leaf nitrogen concentrations as outlined in Section 2.3. In general, tree nitrogen levels were poorly correlated with yellowness index in both years (r values ranging from -0.28 to -0.43 in 2021 and 0.16 and -0.64 in 2023). We also observed an extended retention of greenness in trees that had high N content compared to those with lower N levels. Previous studies have



(a)



(b)

Figure 14: Spatial variation of *yellowness index* over the study period in the test orchard; a) 2021 and b) 2023 datasets. The color bar on the right indicates the yellowness level, with darker shade representing greener trees and lighter shade representing yellower trees..

shown strong correlations between color indices and leaf nitrogen concentration in various plant species. For example, [Lee et al. \(2019\)](#) reported a correlation coefficient of 0.85-0.91 between the SPAD readings and leaf Nitrogen concentration in apples, while [El-Azazy \(2018\)](#) found an R^2 of 0.81 for citrus trees. [Haider et al. \(2021\)](#) observed an even higher R^2 of 0.91 across multiple crops, though their system required crop-specific calibration. Our study's lower correlation might be related to two factors: variable lighting conditions in natural

settings, and a limited range of samples in the lower nitrogen concentration region.

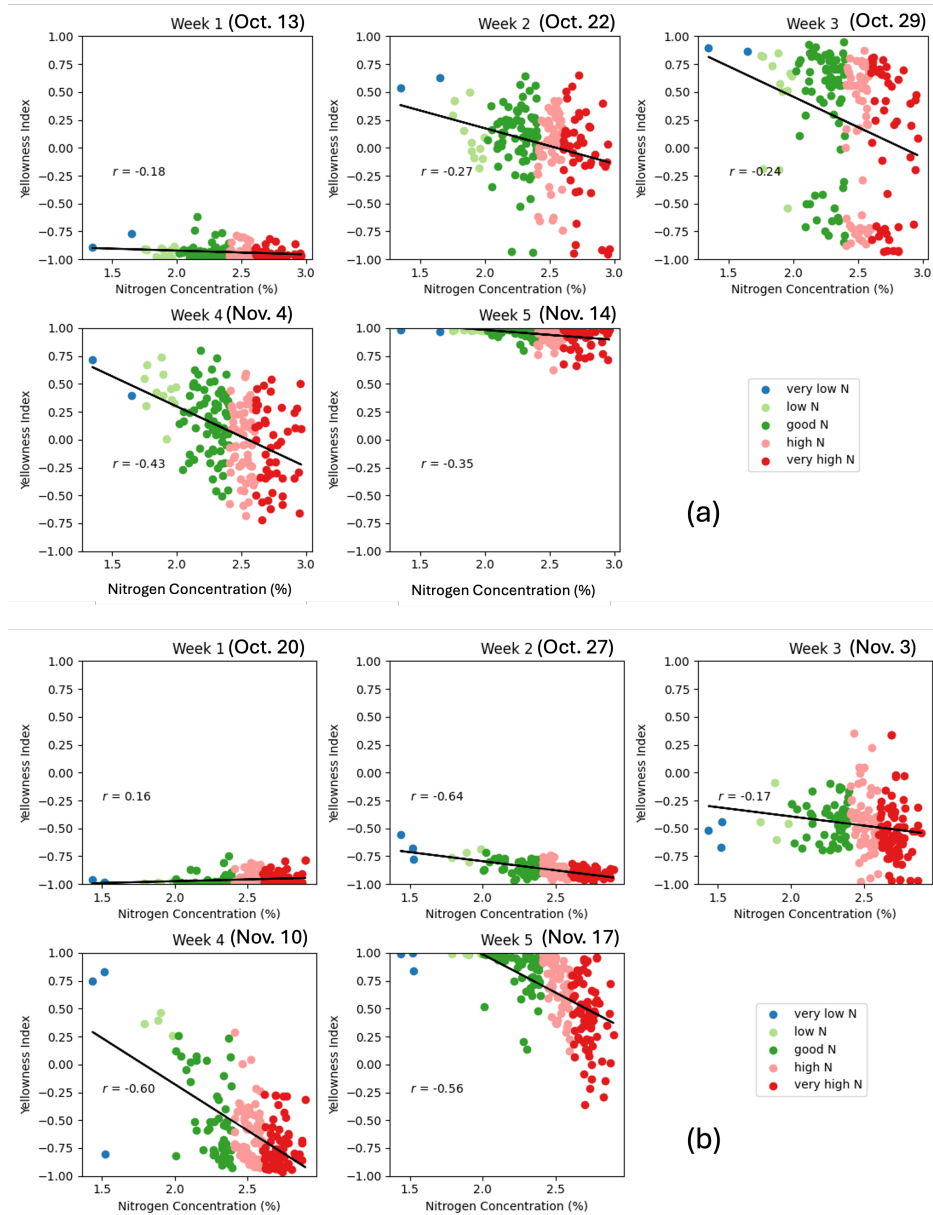


Figure 15: Correlation between N concentration and *yellowness index* over weeks during the fall season of (a) 2021 and (b) 2023 in trees shown with Nitrogen % in the trees. (Very low N ($N < 1.7\%$), Low N ($1.7\% < N < 2.0\%$), Good N ($2\% < N < 2.4\%$), High N ($2.4\% < N < 2.6\%$), Very high N ($N > 2.6\%$). The dates on the plots show the date when the data were collected in 2021 and 2023.

The variability among trees in leaf nitrogen concentration and yellowness index is presented in Figure 16 (a – week 4 of 2021; b – week 5 of 2023). In both plots, red ellipses

highlight areas of the field with higher leaf N and black ellipses represent areas with lower leaf N. In both plots the area with lower leaf Nitrogen has higher yellowness indices in the left plots and vice versa.

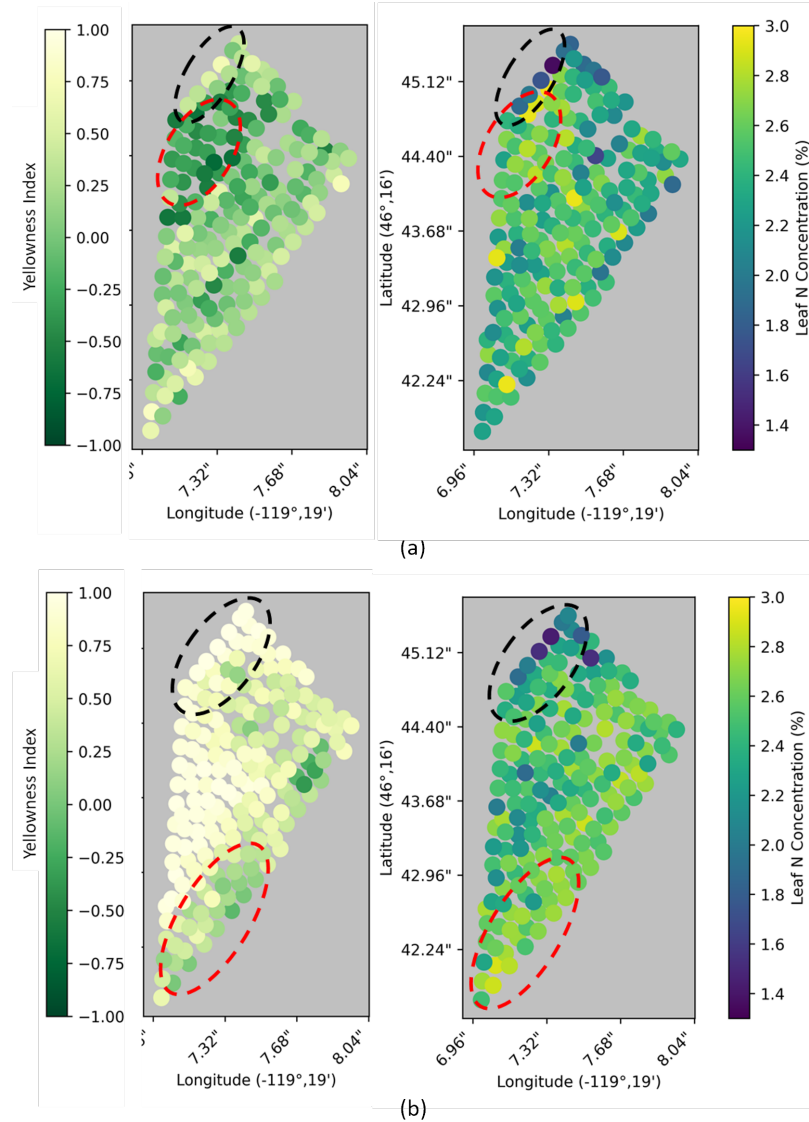


Figure 16: *yellowness index* (left plots) variation with leaf nitrogen concentrations (right plots) in (a) week 4 of 2021, and (b) week 5 of 2023. The color bars on the left and right show the values of *yellowness index* and leaf nitrogen concentrations. The red ellipses show the sample areas with higher nitrogen concentrations, and the black ellipses show areas with lower nitrogen concentrations.

The results from the one-way ANOVA suggested that a significant difference between the group means existed in weeks 1, 3, and 4 of 2021 and weeks 2, 4, and 5 of 2023,

at a significance level of $p < 0.05$. (Table 1). To identify which specific nitrogen level trees differed, a subsequent Tukey HSD test was performed. The columns labeled "Group 1" and "Group 2" show the pairs of trees with those nitrogen levels exhibited significant differences during each week. Each row in the table represents a significant difference in group means between the values in the "Group 1" and "Group 2" columns for the specified week. Significant differences in *yellowness index* between trees with different nitrogen levels were most prominent during weeks 2 and 4 in 2023 and week 4 in 2021.

Table 1: Post-hoc analysis (Tukey test) between trees at different N concentrations when divided into 3 and 5 classes based on leaf Nitrogen concentrations at a) 2021 and b) 2023. The given rows showed significant differences between Group 1 and Group 2 in the column during the given week at a significance level of $p < 0.05$.

Weeks	Year			
	2021		2023	
	Group 1	Group 2	Group 1	Group 2
Week1	Low	Very High		
Week 2	-	-	Very Low	Good
			Very Low	High
			Very Low	Very High
			Low	Good
			Low	High
			Low	Very High
			Good	High
			Good	Very High
Week 3	Low	Very High	-	-
	Good	Very High		
Week 4	Low	High	Very Low	Low
	Low	Very High	Very Low	High
	Good	High	Very Low	Very High
	Good	Very High	Low	Good
			Low	High
			Low	Very High
			Good	High
			Good	Very High
Week 5	-	-	Very Low	Low
			Very Low	Good
			Very Low	High
			Very Low	Very High

While this study suggested a generally lower correlation, there were some weeks in which the correlations were moderate (0.4-0.6), indicating that there may be specific times when trees with different nitrogen concentrations display different *yellowness indices*. Capturing

data during these periods could be useful in identifying trees at different nitrogen levels more effectively. To establish the appropriate timing for accurate and robust *yellowness index* assessment, various factors might need to be considered, such as temperature, growing degree days, precipitation, among others. However, it should be noted that, overall, the correlation remained poor, which suggests that other factors—such as differences in vigor of the trees, irrigation, or the presence of other nutrients—could also have contributed to the variation in *yellowness index*. By identifying these critical time points (in terms of days after full bloom or growing degree days) when significant differences in leaf color occur between trees at different nitrogen concentrations, the yellowness index measured could potentially be used for accurately assessing tree nitrogen status.

The results from this study demonstrated that a machine vision system could be used to identify differences in the yellowing patterns of trees. The outcomes and methodologies of this study offer a means to quantify tree color that could be used to determine tree nitrogen levels, which are crucial factors in guiding fertilizer application to individual trees. However, the system relies on a machine vision system which is susceptible to variations in external lighting conditions. Nevertheless, recent advancements in machine vision sensors have addressed low-light conditions using innovative techniques such as high dynamic range (Zhang et al., 2020, 2021) and Adversarial Networks(Chen et al., 2018). In addition, deep learning methods have notably enhanced imaging system resilience to diverse lighting environments(Li et al., 2021a,b). The algorithm employed in this study relies on labeled data for initially training the model to differentiate yellow and green points on trees, necessitating manual inputs. It's important to note that this algorithm might require further calibration between different years and across tree varieties for optimal performance.

4. Conclusion and Future Work

Leaf Nitrogen concentration is one of the critical factors that determines the yield and quality of fruits and the overall health of apple trees. Growers often rely on different visual

cues including the canopy color for assessing plant health and nitrogen needs. This study presented a machine vision-based approach for quantitatively assessing tree canopy color and utilizing the color during transitional period in the fall (when the leaves change color from green to yellow during senescence) to assess N status in trees. Specifically, this study segmented the test tree canopies in an outdoor environment with natural background using 3D point clouds, identified yellow and green regions in the canopy using a gradient boost model, and used a metric called *yellowness index* to quantify the canopy color. It was found that the trees notably began transitioning in color around the 29th week following full bloom in both years the test was conducted. The trees with lower and higher nitrogen showed significant differences between the *yellowness indices* during week 4 (Around November 4) in 2021 and week 2 (October 27) and week 4 (November 10) in 2023. The difference in these dates signifies the importance of factors such as temperature, humidity, and growing degree days during different years in predicting optimal window of estimate *yellowness index* for tree nitrogen levels assessment. Overall, the findings from this study can be summarized as:

1. A machine vision-based system can be used to segment yellow and green foliage in apple trees in outdoor orchard environments. A metric *yellowness index* was defined to quantify the status of tree foliage color, which was estimated with a R^2 value of 0.72 using a gradient boost classifier model.
2. The *yellowness index* of the trees was found to be correlated with the leaf nitrogen levels in the trees during some periods of the study. Trees with different nitrogen levels showed different yellowing patterns. The difference between low and high nitrogen trees were more significant ($p < 0.05$) in week 4 in 2021(31 weeks after full bloom) and 2023 (29 weeks after full bloom).

This study presented a new approach for assessing the color of apple tree canopies and explored its relationship with leaf Nitrogen concentration. This method could be a good alternative to traditional methods like chemical methods, chlorophyll meter, and spectral

analysis of N assessment in apple trees and can give instantaneous results that could be expanded to individual tree level assessment using a ground vehicle or robot. The study also provided critical insights into the fall color changes in apple trees and their relationship with leaf nitrogen concentrations.

One major limitation of assessing leaf nitrogen level using the proposed method is that some years, the tree might freeze early due to rapid decline in temperature and never show the color change. In such cases, it is important to not rely on just a single factor and have a decision support system that takes multiple features as input, making the decision more robust and reliable. The *yellowness index* values along with other commonly used visual features like canopy density, trunk cross-sectional area, and shoot length can be combined into a single robust model and could aid in developing a robust decision support system for efficient fertilization plans tailored to individual tree nitrogen needs.

Acknowledgement

This research was supported by the Washington Tree Fruit Research Commission. Special thanks to David Allan for providing access to the test orchard and for valuable feedback and support during this work.

References

- Aggelopoulou, K., Pateras, D., Fountas, S., Gemtos, T., Nanos, G., 2011. Soil spatial variability and site-specific fertilization maps in an apple orchard. *Precision Agriculture* 12, 118–129.
- Aggelopoulou, K., Wulfsohn, D., Fountas, S., Gemtos, T., Nanos, G., Blackmore, S., 2010. Spatial variation in yield and quality in a small apple orchard. *Precision agriculture* 11, 538–556.

- Ali, M., Al-Ani, A., Eamus, D., Tan, D., 2012. Leaf nitrogen determination using handheld meters, in: Australian Agronomy Conference.
- Arnó, J., Martínez-Casasnovas, J.A., Uribeetxebarria, A., Escolà, A., Rosell-Polo, J.R., 2017. Comparing efficiency of different sampling schemes to estimate yield and quality parameters in fruit orchards. *Advances in Animal Biosciences* 8, 471–476. doi:[10.1017/S2040470017000978](https://doi.org/10.1017/S2040470017000978). publisher: Cambridge University Press.
- Bartlett, P., Freund, Y., Lee, W.S., Schapire, R.E., 1998. Boosting the margin: A new explanation for the effectiveness of voting methods. *The annals of statistics* 26, 1651–1686.
- Brown, J., Paudel, A., Biehler, D., Thompson, A., Karkee, M., Grimm, C., Davidson, J.R., 2024. Tree detection and in-row localization for autonomous precision orchard management. *Computers and Electronics in Agriculture* 227, 109454.
- Campbell, R.J., Mobley, K.N., Marini, R.P., Pfeiffer, D.G., 1990. Growing conditions alter the relationship between spad-501 values and apple leaf chlorophyll. *HortScience* 25, 330–331.
- Chen, Y.S., Wang, Y.C., Kao, M.H., Chuang, Y.Y., 2018. Deep photo enhancer: Unpaired learning for image enhancement from photographs with gans, in: *Proceedings of the IEEE conference on computer vision and pattern recognition*, pp. 6306–6314.
- Cheng, L., 2010. When and how much nitrogen should be applied in apple orchards. *New York Fruit Quarterly* 18, 25–28.
- Cheng, L., Schupp, J., 2004. Nitrogen fertilization of apple orchards .
- Cho, S.E., 2010. Probabilistic assessment of slope stability that considers the spatial variability of soil properties. *Journal of geotechnical and geoenvironmental engineering* 136, 975–984.

- Dass, B., Rai, A., 2013. Growing degree days (gdd) measurement system to predict plant stages. *Jawaharlal Nehru Krishi Vishwa Vidyalaya Jabalpur 482004 (Madhya Pradesh) India* , 346.
- El-Azazy, A., 2018. Inspect the potential of using leaf image analysis procedure in estimating nitrogen status in citrus leaves. *Middle East Journal of Agriculture Research* 7, 1059–1071.
- Ferguson, I.B., Triggs, C.M., 1990. Sampling factors affecting the use of mineral analysis of apple fruit for the prediction of bitter pit. *New Zealand Journal of Crop and Horticultural Science* 18, 147–152. doi:[10.1080/01140671.1990.10428086](https://doi.org/10.1080/01140671.1990.10428086).
- Fox, R., Piekielek, W., 1978. Field testing of several nitrogen availability indexes. *Soil science society of America journal* 42, 747–750.
- De la Haba, P., De la Mata, L., Molina, E., Agüera, E., 2014. High temperature promotes early senescence in primary leaves of sunflower (*helianthus annuus l.*) plants. *Canadian Journal of Plant Science* 94, 659–669.
- Haider, T., Farid, M., Mahmood, R., Ilyas, A., Khan, M., Haider, S., Chaudhry, M., Gul, M., 2021. A computer-vision-based approach for nitrogen content estimation in plant leaves. *agriculture* 2021, 11, 766.
- James A. Taylor, John-Paul Praat, A. Frank Bollen, 2007. Spatial Variability of Kiwifruit Quality in Orchards and Its Implications for Sampling and Mapping in: *HortScience* Volume 42 Issue 2 (2007) URL: <https://doi.org/10.21273/HORTSCI.42.2.246>.
- Kim, C., Kim, S.J., Jeong, J., Park, E., Oh, E., Park, Y.I., Lim, P.O., Choi, G., 2020. High ambient temperature accelerates leaf senescence via phytochrome-interacting factor 4 and 5 in arabidopsis. *Molecules and cells* 43, 645.
- Kirk, P.L., 1950. Kjeldahl method for total nitrogen. *Analytical chemistry* 22, 354–358.

- Klein, I., Levin, I., Bar-Yosef, B., Assaf, R., Berkovitz, A., 1989. Drip nitrogen fertigation of ‘starking delicious’ apple trees. *Plant and soil* 119, 305–314.
- Lee, D.W., 2002. Anthocyanins in autumn leaf senescence .
- Lee, Y., Kweon, H.J., Park, M.Y., Lee, D., 2019. Field assessment of macronutrients and nitrogen in apple leaves using a chlorophyll meter. *HortTechnology* 29, 300–307.
- Li, C., Guo, C., Han, L., Jiang, J., Cheng, M.M., Gu, J., Loy, C.C., 2021a. Low-light image and video enhancement using deep learning: A survey. *IEEE transactions on pattern analysis and machine intelligence* 44, 9396–9416.
- Li, C., Guo, C., Loy, C.C., 2021b. Learning to enhance low-light image via zero-reference deep curve estimation. *IEEE Transactions on Pattern Analysis and Machine Intelligence* 44, 4225–4238.
- Mahmud, M.S., Zahid, A., He, L., Choi, D., Krawczyk, G., Zhu, H., Heinemann, P., 2021. Development of a lidar-guided section-based tree canopy density measurement system for precision spray applications. *Computers and Electronics in Agriculture* 182, 106053.
- Marschner, H., 2011. Marschner’s mineral nutrition of higher plants. Academic press.
- Murneek, A.E., Logan, J., 1932. Autumnal migration of nitrogen and carbohydrates in the apple tree with special reference to leaves. University of Missouri, College of Agriculture, Agricultural Experiment Station.
- Naschitz, S., Naor, A., Wolf, S., Goldschmidt, E.E., 2014. The effects of temperature and drought on autumnal senescence and leaf shed in apple under warm, east mediterranean climate. *Trees* 28, 879–890.
- Natekin, A., Knoll, A., 2013. Gradient boosting machines, a tutorial. *Frontiers in neuro-robotics* 7, 21.

- Neilsen, D., Hogue, E.J., Neilsen, G.H., Parchomchuk, P., 1995. Using spad-502 values to assess the nitrogen status of apple trees. *HortScience* 30, 508–512.
- Neilsen, D., Neilsen, G., 2002. Efficient use of nitrogen and water in high-density apple orchards. *HortTechnology* 12, 19–25.
- Neilsen, G.H., Neilsen, D., Herbert, L., 2009. Nitrogen fertigation concentration and timing of application affect nitrogen nutrition, yield, firmness, and color of apples grown at high density. *HortScience* 44, 1425–1431.
- Parkin, T., 1993. Spatial variability of microbial processes in soil—a review. *Journal of environmental quality* 22, 409–417.
- Paudel, A., Davidson, J.R., Grimm, C., Karkee, M., 2023. Vision-based normalized canopy area estimation for variable nitrogen application in apple orchards. *Smart Agricultural Technology* 5, 100309.
- Paudel, A., Karkee, M., Davidson, J.R., Grimm, C., 2022. Canopy density estimation of apple trees. *IFAC-PapersOnLine* 55, 124–128.
- Perry, E.M., Davenport, J.R., 2007. Spectral and spatial differences in response of vegetation indices to nitrogen treatments on apple. *Computers and Electronics in Agriculture* 59, 56–65.
- Raese, J.T., Drake, S.R., Curry, E.A., 2007. Nitrogen fertilizer influences fruit quality, soil nutrients and cover crops, leaf color and nitrogen content, biennial bearing and cold hardiness of ‘golden delicious’. *Journal of plant nutrition* 30, 1585–1604.
- Sallato, B., 2017. Leaf tissue analysis. URL: <https://treefruit.wsu.edu/orchard-management/soils-nutrition/leaf-tissue-analysis/>.
- Sanchez, E.E., Khemira, H., Sugar, D., Righetti, T., 1995. Nitrogen management in orchards.

- Spencer, P.W., 1973. Apple leaf senescence: leaf disc compared to attached leaf. *Plant physiology* 51, 89–92.
- Thompson, D., 2017. How to Use Color Spaces to Talk About Color - First Source Worldwide. URL: <https://www.fsw.cc/color-spaces/>.
- Treder, W., Klamkowski, K., Kowalczyk, W., Sas, D., Wojcik, K., et al., 2016. Possibilities of using image analysis to estimate the nitrogen nutrition status of apple trees. *Zemdirbyste-Agriculture* 103, 319–326.
- Umali, B.P., Oliver, D.P., Forrester, S., Chittleborough, D.J., Hutson, J.L., Kookana, R.S., Ostendorf, B., 2012. The effect of terrain and management on the spatial variability of soil properties in an apple orchard. *Catena* 93, 38–48.
- UniversityofArizona, . Nitrogen management guide for apples. URL: <chrome-extension://efaidnbmnnnibpcajpcglclefindmkaj/https://ag.arizona.edu/crop/soils/aznapples.pdf>.
- Wachs, J.P., Stern, H.I., Burks, T., Alchanatis, V., 2010. Low and high-level visual feature-based apple detection from multi-modal images. *Precision Agriculture* 11, 717–735.
- Van der Walt, S., Schönberger, J.L., Nunez-Iglesias, J., Boulogne, F., Warner, J.D., Yager, N., Gouillart, E., Yu, T., 2014. scikit-image: image processing in python. *PeerJ* 2, e453.
- Wang, T., Sankari, P., Brown, J., Paudel, A., He, L., Karkee, M., Thompson, A., Grimm, C., Davidson, J., Todorovic, S., 2023. Automatic estimation of trunk cross sectional area using deep learning. Collaborative Robotics & Intelligent Systems Institute, Oregon State University .
- Wang, Z., Underwood, J., Walsh, K.B., 2018. Machine vision assessment of mango orchard flowering. *Computers and Electronics in Agriculture* 151, 501–511.

- Wulfsohn, D., Aravena Zamora, F., Potin Téllez, C., Zamora Lagos, I., García-Fiñana, M., 2012. Multilevel systematic sampling to estimate total fruit number for yield forecasts. *Precision Agriculture* 13, 256–275. URL: <https://doi.org/10.1007/s11119-011-9245-2>, doi:10.1007/s11119-011-9245-2.
- Ye, X., Abe, S., Zhang, S., 2020. Estimation and mapping of nitrogen content in apple trees at leaf and canopy levels using hyperspectral imaging. *Precision Agriculture* 21, 198–225.
- Zhang, S., Zhang, Y., Jiang, Z., Zou, D., Ren, J., Zhou, B., 2020. Learning to see in the dark with events, in: *Computer Vision–ECCV 2020: 16th European Conference, Glasgow, UK, August 23–28, 2020, Proceedings, Part XVIII* 16, Springer. pp. 666–682.
- Zhang, Y., Guo, X., Ma, J., Liu, W., Zhang, J., 2021. Beyond brightening low-light images. *International Journal of Computer Vision* 129, 1013–1037.
- Zhou, Q.Y., Park, J., Koltun, V., 2018. Open3d: A modern library for 3d data processing. arXiv preprint arXiv:1801.09847 .